Mixed Ionic-Electronic Transport in Polymers

Bryan D. Paulsen, ¹ Simone Fabiano, ² Jonathan Rivnay ^{1,3}

¹Department of Biomedical Engineering, Northwestern University, Evanston, Illinois 60208, United States

²Laboratory of Organic Electronics, Department of Science and Technology, Linköping University, SE-601 74 Norrköping, Sweden

³Simpson Querrey Institute, Northwestern University, Chicago, Illinois 60611, United States

Keywords

polymer electrolytes, polyelectrolytes, conjugated polymers, conducting polymers, mixed conductor, mixed transport

Abstract

Polymeric mixed ionic-electronic conductors (MIECs) combine aspects of conjugated polymers, polymer electrolytes, and polyelectrolytes to simultaneously transport and couple ionic and electronic charge, opening exciting new applications in energy storage and conversion, bioelectronic, and display technologies. The many applications of polymeric MIECs lead to a wide range of transport conditions. Ionic and electronic transport are directly coupled through electrochemical doping, while the mechanisms of ionic and electronic transport depend on distinctly different chemical functionality, (macro)molecular structure, and morphology. Despite this, ionic and electronic transport are surprisingly tunable, independent of one another. We review the various types of polymeric MIECs, the mechanisms of ionic and electronic charge transport across conditions, and the interrelations between two, with special emphasis on the unique aspects of polymeric MIEC transport phenomena.

Introduction

Initially, electronically conducting polymers and ionically conducting polymers were developed separately. Electronically conducting polypyrrole was discovered and reported 1963 (1), though it was not until the independent discovery and report of electrically conducting polyacetylene in 1977 that electrically conducting conjugated polymers (CPs) received wider attention (2). Around roughly the same time, poly(ethylene oxide) was found to be capable of dissolving salts (3) and displaying significant ion conduction (4). Both systems were very quickly recognized to have promise in electrochemical applications, and thus it was only a matter of time before polymeric

materials were purposefully designed to leverage both electronic and ionic conduction simultaneously.

Polymer mixed ionic electronic conductors (MIECs) were explicitly recognized and studied beginning in the late 1980's as potential battery electrodes (5). Since then a robust field of organic mixed ionic electronic conductors has emerged (6), amongst which polymeric MIECs are the most successful. Being 'soft' solids, polymeric MIECs are mechanically, electrically, and chemically responsive, in unique ways compared to traditional inorganic MIECs (6). Today polymer mixed conductors have been employed in light emitting electrochemical cells (7), actuators (8), neuromorphic devices (9), bioelectronics (10), organic electrochemical transistors (11), iontronics (12), thermoelectrics (13), supercapacitors (14), battery electrodes (15), and electrochromics (16), to name a few. Polymeric MIECs are so broadly applicable due ionic-electronic interactions that allow them to store and transduce (ionic and electronic) charge and signals, respectively.

It is instructive to look to the more established fields of ionic transport in polymer electrolytes/polyelectrolytes and electronic transport in doped organic semiconductors. However, the same ionic-electronic interactions that make polymeric MIECs attractive, complicate mixed transport. The numerous insightful studies of mixed transport in polymers, are spread across several decades and multiple disciplines, thus we draw important connections across the literature to assemble a complete picture of present body of knowledge of mixed transport in polymeric materials. Here in, we describe the ion and electronic transport in polymeric MIECs from the dry to gelled state, with an emphasis on the deviations from the behavior of simple electronic or ionic conductors. Further we highlight the unique synergetic effect on thermally driven charge transport.

1. Ionic Transport

The understanding of ionic transport in polymeric MIECs is dependent on the extensive work done studying electrically insulating polymer electrolytes and polyelectrolytes, Figure 1a & b. In particular, the following draws heavily on some classic texts(17, 18) and excellent recent reviews (19, 20), To survey ionic transport in polymeric MIECs it is worthwhile to consider what chemical functionality allows for ions to dissolve in polymers, what phenomena drive ionic transport, the macromolecular motion that allows/facilitate said ionic transport, and various compositional environments in which ionic transport in polymeric MIECs occurs.

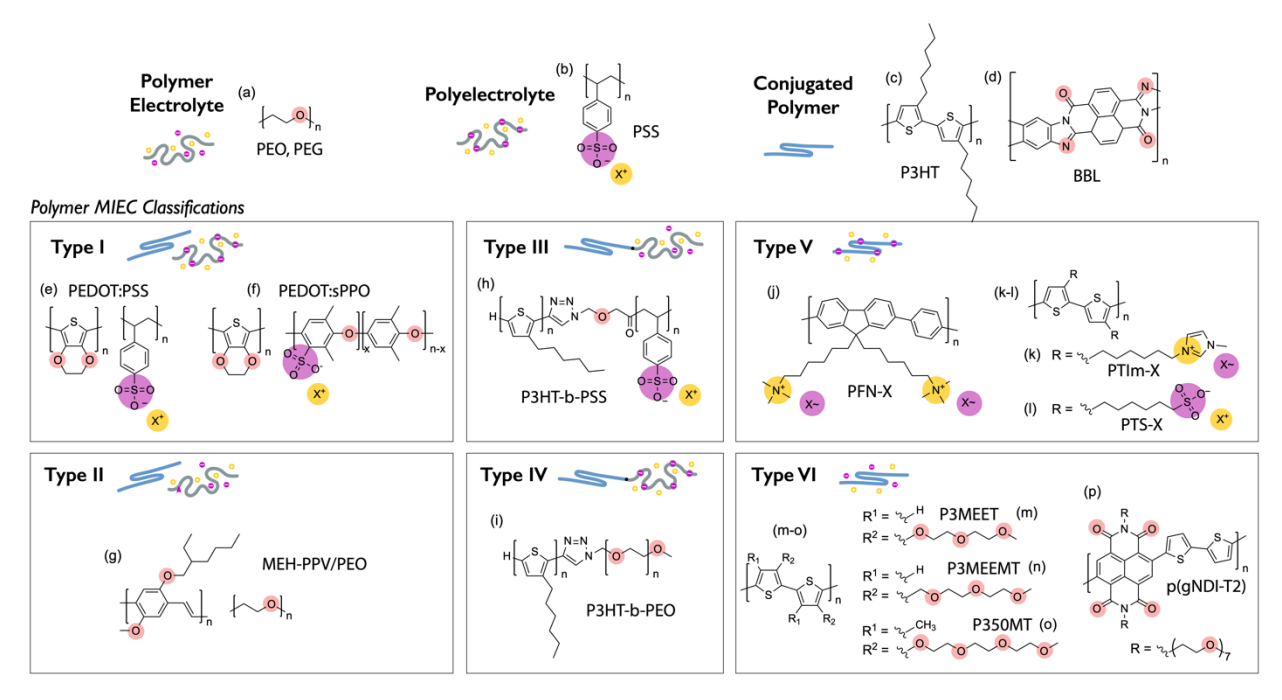


Figure 1. Chemical structures of representative (a) polymer electrolytes, (b) polyelectrolytes, (c & d) conjugated polymers (CPs), (e & f) type i CP/polyelectrolytes composites, (g) type ii CP/polymer electrolytes blends, (h) type iii CP-b-polyelectrolytes block copolymers, (i) type iv CP-b-polymer electrolytes block copolymers, and (j-l) type v conjugated polyelectrolytes (m-o) type vi conjugated polymer electrolytes; with anions, cations, and coordinating groups highlighted in purple, yellow, and red, resepectively.

1.1. Ion solvation

For a polymer to conduct ions it must be able to dissolve a salt (i.e. a reduction of Gibbs free energy of the salt dissolved in the polymer compared to the pure salt crystal). Poor solvation in polymeric MIECs manifests on the device level as ion injection and transport barriers, and poor ionic-electronic coupling (e.g. charge storage or doping). In typical electrolytes, solvation of ions arises by hydrogen bonding in protic, high dielectric constant electrolytes (e.g. water) or coordination to dipole containing functional groups in aprotic electrolytes (e.g. ether oxygens in tetrahydrofuran), Figure 2a & b. The most common solid polymer electrolytes leverage periodically repeating ether oxygen groups to coordinate and solvate cations, Figure 1a & 2c, while anions are present but unsolvated. Alternatively, the polymer can be a component of the salt itself, paired with charge balancing counter ions, Figure 1b & 2e, as in the case of ionomers (<10% of the repeat units bear ionic charge) or polyelectrolytes (>10% of the repeat units bear ionic charge). Typical examples of polymer electrolytes and polyelectrolytes are polyethylene oxide (PEO) and polystyrene sulfonate (PSS), respectively (Figure 1a & b).

Traditional CPs, Figure 1c & d, tend to have low dielectric constants, lack (a high density of) ion coordinating functional groups, often contain long nonpolar alkyl side chains, and thus do not readily dissolve most salts. Polymeric MIECs overcome this via the incorporation of ionic charge (polyelectrolytes) or coordinating groups (polymer electrolytes), Figure 2d &f. These can be present as side chains of the polymer backbone, covalently linked blocks, or distinct polymer electrolytes/polyelectrolytes which the CP has been composited with or templated on. This naturally gives rise to a polymer mixed conductor taxonomy of (i) CP/polyelectrolyte blends, (ii) CP/polymer electrolyte blends, (iii) CP-b-polyelectrolyte block copolymers, (iv) CP-b-polymer electrolyte block copolymers, (v) conjugated polyelectrolytes, (vi) conjugated polymer electrolytes, Figure 1, (6).

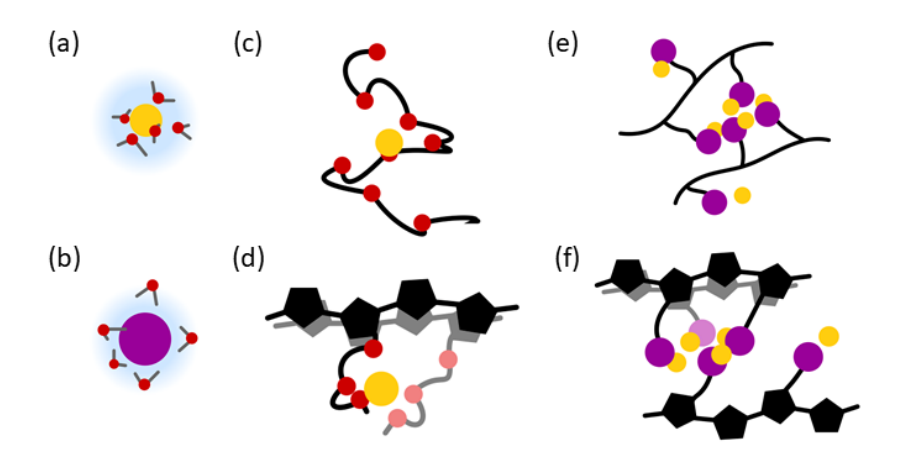


Figure 2. Ion Solvation: Illustrations of (a) cation and (b) anion solvation by water in aqueous electrolytes, cation coordination by ether oxygens in (c) non-conjugated and (d) conjugated polymer electrolytes, and ion-pairing and aggregation in (e) non-conjugated and (f) conjugated polyelectrolytes. The Cations, anions, and oxygens are displayed in yellow, purple, and red, respectively.

For polyelectrolyte MIECs (type i, iii, and v), the tethered ionic charge requires counterbalancing ions to maintain charge neutrality. Fixed ions are associated with oppositely charged counterions producing ion pairs, and ion pairs are energetically predisposed to cluster and aggregate, Figure 1e & f, (21). In type vi conjugated polyelectrolytes the ionic moieties are tethered via side chains (often alkyl in nature) to a rigid conjugated backbone, Figure 1d and 2k-m. The rigidity of the conjugated backbone and the energetic preference for π - π interchain interactions limit the degree

of aggregation/clustering. Generally, ionic aggregates are confined to the lamellar spacing between pi-stacked conjugated backbones (22–24).

Type ii, iv, and vi polymer electrolyte MIECs most often employ (poly/oligo)ether chains, blocks, or sidechains, respectively. Ion solvation requires sufficient coordination sites, suitably spaced to allow chain conformation around the ion. In the linear polyethers, this ideal spacing is two carbons between each ether oxygen, as found in PEO, Figure 1a. Alkali metal cations can reside in a PEO helix, coordinating with several ether oxygens (on average six in the case of Li+), Figure 2c. Due to the low dielectric constant these dissolved ions are poorly screened and can also associate into multi ion aggregates directly as contact clusters, or indirectly as solvent (chain) separated clusters. In PEO, anion coordination is negligible, as such, small halide ions are poorly soluble while larger or polarizable anions (e.g. TFSI) improve solubility (18).

In type i-iv polymeric MIECs (Figure 1f-j) conjugated and ionic/ion-coordinating macromolecular components tend to phase segregate into CP rich domains and polyelectrolyte/polymer electrolyte rich domains, with ion dissolution occurring primarily in the latter. In type v and vi polymeric MIECs (Figure 1k-q) ionic/ion-coordinating groups are evenly distributed along the polymer and cannot naturally phase segregate. Due to phase segregation, type i-iv polymer MIECs tend to present compositional heterogeneity on the 10s -100s nm length scale, while lengths scales compositional heterogeneity in type v and vi is determined by the side chain length (2-4 nm). Often, polymeric MIECs are semi-crystalline, and the relative distribution of ions between the amorphous and crystalline domains is an open question (25, 26).

In polymer mixed conductors, ions can also interact with electronic charge. On the whole, electronic charge (holes or electrons) require a counterbalancing dopant (anion or cation) to maintain charge balance. In polyelectrolyte MIECs (i,iii,v), these can be some fraction of the fixed ionic charge on the polyelectrolyte. In type ii, iv, and vi polymer mixed conductors dopant ions are separately dissolved ionic species. Localized (trapped) electronic charge present as discrete sites for ionic-electronic coordination (M. Matta M, R. Wu R, B.D. Paulsen, A. Petty, R. Sheelamanthula, et al., manuscript in review). Conversely, delocalized electronic charge leads to a large increase in the dielectric constant (27) that works to screen particular ionic-ionic and ionic-electronic associations. In phase separated polymer mixed conductors (type i-iv) the coordination between ionic and electronic charge can accumulate at the interface between the

polyelectrolyte/polymer electrolyte rich domains and the conjugated polymer rich domains (28, 29).

1.2. Ion Drift and Diffusion

lonic transport occurs in response to electric field (drift/migration) and concentration gradient (diffusion), and discounting convection, can be considered a summation of Ohm's law and Fick's law. For dilute systems in one dimension, the current density (J_{ion}) due to ionic transport can be described as:

$$J_{ion} = \sum \left[e|z_i| n_i \mu_i \frac{d\Phi}{dx} + ez_i D_i \frac{dn_i}{dx} \right]$$

were e is the elementary charge, ϕ is the potential; and z_i is the charge, n_i is the number density μ_i is the mobility, and D_i is the diffusion coefficient of each ionic species. It follows that $\sigma_{ion} = \Sigma[e|z_i|n_i\mu_i]$ is the ionic conductivity. In dilute conditions, n_i is easily convertible to the anion or cation concentration (c_i), and D_i and μ_i , are interconvertible with the Nersnst-Einstein:

$$D_i = RT\mu_i$$

where R is the gas constant. However, assumptions of infinite dilution do not hold in polymer MIECs. Ion interaction can produce neutral ion pairs (that can diffuse but do not migrate), net charged ion triplets, and larger clusters or aggregates that can be neutral or charged. Thus raw anion and cation concentrations are not informative, and absent known concentrations of each ion and multi-ion species, anion and cation thermodynamic activities should be used. Additionally, depending on local pH there may be non-negligible proton, hydronium, or hydroxide transport in hydrated or aqueous systems.

Given this complexity, ionic transport in polymer MIECs is often quantified as simple σ_{ion} or molar fluxes. When diffusion coefficients or mobilities are reported, they should be considered "apparent" of "effective", unless rigorously proven otherwise. In certain systems it can be helpful to consider ionic transport using Maxwell-Stefan diffusion (20) or in terms of effective salt diffusion coefficient and transference number (19).

While in typical electrolytes electroneutrality requires the local cation and anion concentrations to be equal, this is not the case in polymeric MIECs as holes or electrons can accumulate to counter balance excess anions or cations.

$$F \sum z_i c_i + e n_{holes} - e n_{electrons} = 0$$

where F is Faraday's constant, c_i is the individual ion concentrations, and n is the number density of electrons or holes. Thus, ionic transport in polymer MIECs can give rise to independent anion and cation concentration gradients (30) which is leveraged in light emitting electrochemical cells (LEECs) (31).

1.3. Chain Motion

Solvated ion motion is necessarily coupled to the motion of the surrounding media. In liquid electrolytes, the bulk solvent molecules are highly mobile and reorganize around the ion and its solvation shell as they move together (i.e. vehicle transport), which manifests as a drag on ion motion that is proportional to the electrolyte viscosity. In polymers, ionic transport is similarly connected to motion of the surrounding macromolecules.

Except for low molecular weight oligomers, the solvating shell of coordination groups or ionic moieties covalently bound to the polymer cannot transport with the ion (i.e. no vehicle transport). Thus, the solvation shell is continually reforming as ions move between coordination sites through local motion of the polymer chains. On short time and length scales, polymer segmental motion can be described as an unentangled chain using the Rouse or Zimm models, while on longer time and length scales the motion of an entire entangled polymer chain can be described using the reptation model (32). Uncoordinated ions (e.g. anions in PEO) still depend on chain motion to move through the available free volume of the polymer. Due to this dependence on chain motion, crystallinity is detrimental to ionic transport.

When considering chain coupled ion motion, it is instructive to consider the polymer persistence length (ℓp), which describes the length below which the polymer acts like a rigid rod. For example, ℓp for PEO is only 4 Å (Figure 1a) (32, 33), thus a single chain can conform around a cation and provide multiple sites for cation-ether oxygen coordination. Polystyrene has a $\ell p \approx 7.3$ Å (32), while PSS (Figure 1b) has a $\ell p \approx 12$ Å (34), as the aggregation of ion pairs results in longer "rigid"

segments of polymer. The PEO ℓp is sufficiently short (i.e. the polymer is sufficiently flexible) such that segmental motion occurs close to the scale of individual ion-coordinating ether oxygens, allowing the cation to move while maintaining a highly coordinated solvation shell. PSS chains are not so flexible as to allow the individual motion of coordinating sulfonate ions, but still flexible enough to bring neighboring ion aggregates in and out of close proximity with each other, allowing ion hopping.

Polymeric MIECs contain a high degree of conjugation imparting increased chain rigidity. For example, regio regular P3HT (Figure 1c) in dilute solution displays a $\ell p = 29$ Å, over seven times that of PEO (35). In the solid state, this increases to a $\ell p = 49$ Å and $\ell p = 75$ Å for amorphous and crystalline chains, respectively (36). Thus conjugated chains are not able to conform themselves to particular ions, with limited local segmental motion to assist ion motion. Fluctuations in the dihedral angle between repeat units (e.g. the ethylenedioxy ring on PEDOT) may impart some small ability for coordinating sites to reorient in response to adjacent cations, particularly in amorphous domains (37, 38). As with ion solvation, in phase separated systems (type i-iv) segmental motion in the non-conjugated polyelectrolyte/polymer electrolyte rich domains promotes ionic transport. For nominally homogenous type v and vi polymer MIECs, the local motion of the ionic or ion-coordinating side chains enables ion motion.

Because of the dependence of ionic transport on polymer motion, the temperature dependence of σ_{ion} often follows the same functional dependence as the Vogel-Fulcher-Tammann (VFT) formulation of viscosity near a materials glass transition temperature, T_g (39).

$$\sigma_{ion} = \sigma_0 e^{\left(\frac{-B}{R(T-T_0)}\right)}$$

While this is an empirical model, T_0 is generally related to T_g by a constant offset. Below (18) and far above (19) T_g , a simple Arrhenius dependence captures the temperature dependence of ionic conductivity (40).

$$\sigma_{ion} = \sigma_0 e^{\left(\frac{-E_a}{RT}\right)}$$

Where E_a is the activation of energy of the ionic transport. In traditional CPs, the VFT relationship must be modified to account for the applied potential and the solubility mismatch of ions with CPs (41).

Despite the importance of thermal transitions in rationalizing ionic transport, the thermal properties of polymeric MIECs are not fully understood. In conjugated polyelectrolytes (v), melt and glass transitions are counter-ion dependent (24). In type vi systems thermal transitions are often not observed, despite clear crystallinity as assessed by X-ray scattering. In random copolymers of oligoethylene glycol and alkyl sidechain monomers, an oligoethylene glycol fraction of 5% is sufficient to suppress all measurable thermal transitions, despite significant crystallinity being retained (P.A. Finn, I.E. Jacobs, J. Armitage, R. Wu, B.D. Paulsen, et al., manuscript in review). In similar homopolymers, a glass and multiple melt transitions are apparent when a methyl group separates the polythiophene backbone and the first sidechain ether oxygen. Absent the methyl spacer, two glass transitions but no melting transitions were observed, despite both showing crystallinity via diffraction(42). It is possible that the enthalpy of melting (ΔH_m) is suppressed in these systems, or that the T_m is shifted beyond the degradation temperature.

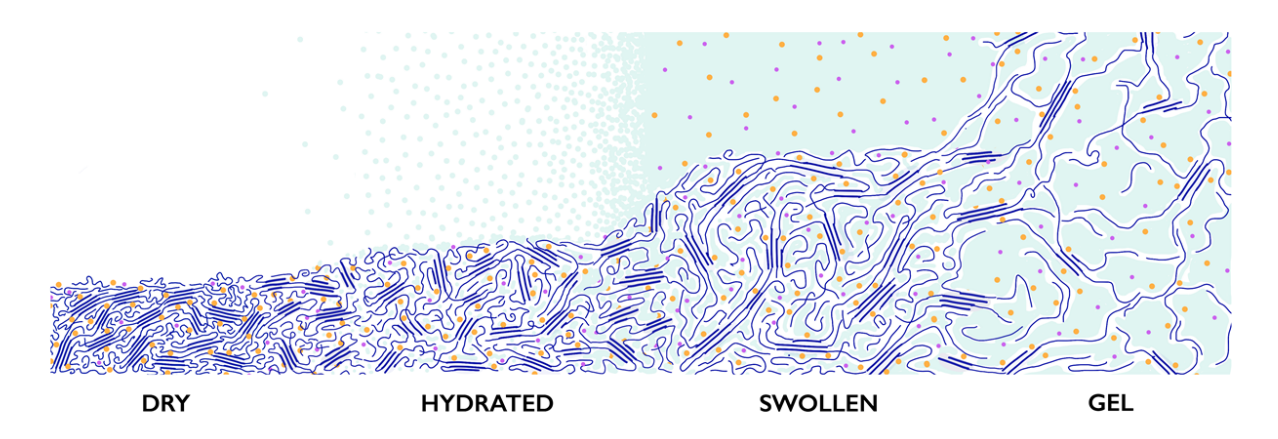


Figure 3. Illustration of the dry to hydrated to electrolyte swollen to gelled continuum of polymeric MIECs.

1.4. Ionic Transport Environments

There are four general ionic transport conditions to consider: dry, hydrated, swollen by a contacting liquid electrolyte, and (hydro)gelled, Figure 3. These conditions arise from varied applications of polymeric MIECs, and each case presents unique characteristics that influence ionic transport.

1.4.1. Dry Ionic Transport

The dry condition consists simply of the mixed conducting polymer and dissolved ions, lacking liquid solvent molecules from ambient vapor or a contacting liquid electrode. These can be "closed" systems with a fixed total composition (e.g. LEECs), or "open" systems in contact with any ion sink/source (e.g a solid polymer electrolyte) with a dynamic total composition (e.g. solid state battery electrodes). In both cases, ionic transport is dependent on chain fluctuations, and extended conjugation is detrimental to ionic transport. Microphase separated materials with flexible non-conjugated chains/blocks show the highest dry σ_{ion} (39, 43–45). In type iv P3HT-b-PEO (Figure 1i), $\sigma_{ion} \sim 5 \times 10^{-4} \text{ S cm}^{-1}$ at 90°C, is on par with pure PEO when normalized by ether oxygen content (39, 44, 45), indicating good connectivity between ion coordinating sites (46). Type vi conjugated homopolymer electrolytes (P350MT, Figure 1o) with oligoethylene glycol side chains display a decreased σ_{ion} of 4 x 10⁻⁵ S cm⁻¹ at similar temperatures, due to decreased segmental motion from extended backbone rigidity (47), which likely manifests as a loss of coordination site connectivity (46).

Ion coordination "pins" chains, decreasing their fluctuations, increasing T_g with increasing ion concentration. For example, the T_g of the PM350T (type vi, Figure 1o) increases ~90 C from neat to a salt loading of 0.35 cation per sidechain ether oxygen (47). In addition, ion-ion interactions lead to a negative dependence of ion mobility on ion concentration. These compounding effects cause σ_{ion} to rise with initial addition of salt, peak below 0.1 cation per ether oxygen, and decrease with additional salt in type ii and vi polymeric MIECs (Figure 4a) (42, 43, 47) similar to PEO (19).

In the dry state, type vi conjugated polyelectrolyte MIECs (Figure 1j-l) display very low σ_{ion} (~10⁻¹¹ S cm⁻¹) (40, 48–50), as strong ion-ion interactions leave only ~0.1% of ions mobile (49), and the limited segmental motion due to conjugated backbone rigidity requires long hops between aggregates with large activation energies (0.8-1.6 eV) (40, 48, 49). Tripling the ion containing side chain density on polyfluorene based conjugated polyelectrolytes (Figure 1j) halves the activation energy and increases σ_{ion} by an order of magnitude (~10⁻¹⁰ S cm⁻¹) (49), presumably due both to an increase in mobile ions and a decrease in hopping distance between ion aggregates.

In electrically insulating polymer electrolytes, non-volatile additives (crown ethers, tetraglyme, ionic liquids, etc) have been shown to improve ionic transport by plasticizing the polymers (51),

and creating a mobile solvation shell, *a la* vehicle transport. Initial studies of polymeric MIECs with ionic liquids (52, 53), sorbitol (54, 55), and crown ethers (56) have been promising.

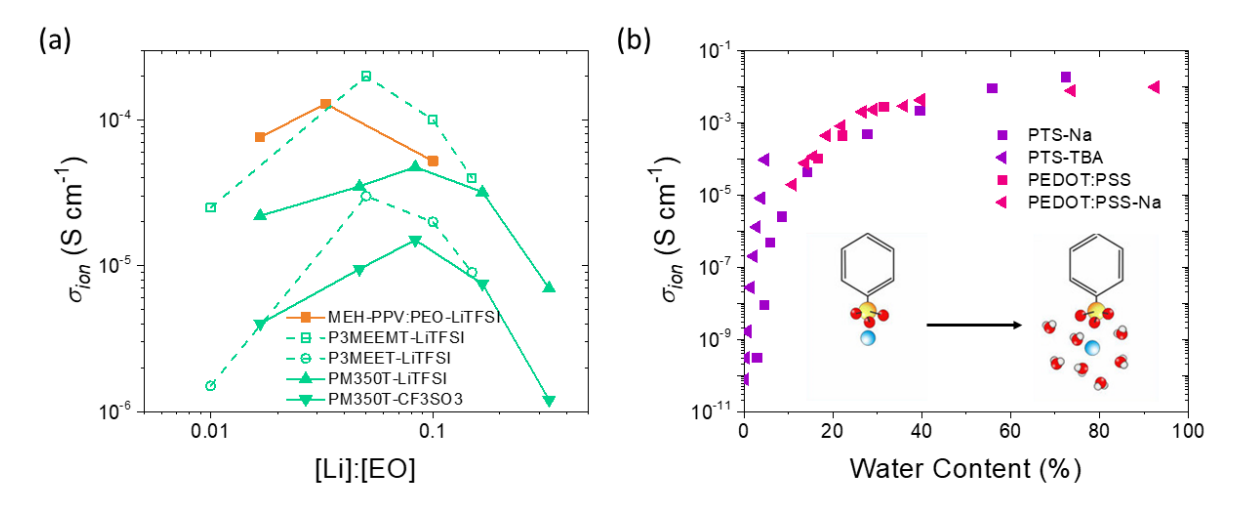


Figure 4. Ionic conductivity dependence on (a) cation concentration (cation per ether oxygen) in dry type ii and vi polymer electrolyte based MIECs, and (b) water content in hydrated type ii and vi polyelectrolyte based MIECs. Panel (a) highlights the general effect of ion-ion interactions limiting σ_{ion} as the cation:ether oxygen ratio approaches 0.1. The inset in panel (b) illustrates the dissociative effect of hydration, leading to dramatic increases in σ_{ion} .

1.4.2. Hydrated Ionic Transport

Hydration has a tremendous effect on ionic transport in polymer mixed conductors. Many polymer MIECs (especially i, iii, v) show such low σ_{ion} in the dry state that they can be considered as simply electrical (semi)conductors due to strong ion association with the polymer and limited chain motion. With hydration, water plasticizes chains, increasing chain motion, and begins to solvate the ions, partially displacing the polymer in the cation solvation shell (M. Matta M, R. Wu, B.D. Paulsen, A. Petty, R. Sheelamanthula, et al., manuscript in review). In conjugated polyelectrolytes, water dissociates the counterion. A sufficient degree of hydration produces a mobile solvation shell of water, allowing vehicle transport. At room temperature, conjugated polyelectrolytes (vi) σ_{ion} spans 7-8 orders of magnitude depending on degree of hydration, Figure 4b (40, 50). PEDOT:PSS (type i) also shows similarly large increases in σ_{ion} with increased hydration, and the degree of hydration in both can be quite large, 70-90 wt% at 90% RH (50). At high levels of hydration, temperature dependent σ_{ion} deviates from VTH or Arrhenius behavior (40).

The σ_{ion} of type i materials with high water content is quite high (10⁻³-10⁻² S cm⁻¹, Figure 5) (40, 50, 57–59). These conductivities approach that of the equivalent aqueous electrolytes. As many polymeric MIECs incorporate HPSS, parallel proton transport via the Grotthuss mechanism likely becomes significant in the highly hydrated state (60).

1.4.3. Electrolyte Swollen Ionic Transport

Many applications require polymeric MIECs to be in contact with liquid electrolytes (10, 11, 14, 16). This complicates the description of transport as ions and solvent are now in a concentration and electrochemical potential dependent equilibrium between the contacting liquid electrolyte and polymer MIEC (61). This is most obvious in potential dependent swelling of polymeric MIECs in response to electrochemically induced electronic charge. In this environment many marginal polymeric MIECs that minimally solvate/transport ions become surprisingly effective mixed conductors. As an example, the type vi material p(g2T-TT) only passively swells ~10% when in contact with aqueous NaCl, independent of electrolyte concentration. However, upon the application of an oxidizing potential, p(g2T-TT) reversibly swells an additional 42 to 86% (61). This exemplifies the important contribution of electronic charge in ion solvation/coordination. In a similar material with roughly double the density of oligoethylene glycol side chains, the reversible swelling in response to electrochemical potential is increased to ~300% and can exceed 1000%, though irreversibly (62). This electrochemical potential dependent polymeric MIEC swelling is intuitively expected to lead to large changes in σ_{ion} , though this has yet to be directly experimentally verified.

In traditional hydrophobic CPs electrochemical potential dependent swelling manifests as voltage switchable semiconductor to mixed conductor behavior. In the neutral state (absence of electronic charge) hydrophobic CPs do not dissolve ions or water, however once electronic charge is present it is energetically favorable (required) that dopant ions are present, thus the film swells with electrolyte. The electrochemical potential necessary for this to occur is not simply connected to the HOMO level of the CP, but includes an ion dependent overpotential (63), that increases with decreasing ion polarizability, and is inversely proportional with ion miscibility in the CP (41). In true MIEC polymers that are sufficiently able to solvate ions, this overpotential is effectively zero, and the onset of electrochemical potential dependent swelling tracks with HOMO/LUMO level positions.

Peculiarly, the rigid backbone ladder polymer BBL (Figure 1d), passively swells ~10% when in contact with an aqueous electrolyte, and swells ~100% upon application of a reductive potential with little apparent overpotential (J. Surgailis, A. Savva, V Druet, B.D. Paulsen, R.Wu., et al., manuscript in preparation). This is quite unexpected due to the low density of ion coordination sites (carbonyl groups) and large \$\ell\$p of BBL (~1530 Å) (64) would imply the inability of local segmental motion to assist ionic transport. BBL may have sufficient free volume to allow ion and water penetration, and due to its rigidity may form a unique rigid rod gel network allowing a high degree of swelling, however this phenomenon deserves further study.

As with highly hydrated systems, polyelectrolyte based MIECs in contact with liquid electrolytes display facile ionic transport. Across a variety of ions, PEDOT:PSS σ_{ion} shows the same concentration dependence as liquid electrolytes (65). PEDOT:PSS moving front experiments revealed ion mobilities ions on par with aqueous electrophoretic mobilities (66). As excessive swelling can be detrimental to device stability, cross-linkers are often employed to decrease polymeric MIEC swelling. In crosslinked PEDOT:PSS the ionic mobility was decreased by an order of magnitude, in keeping with the expected swelling-conductivity relationship (66).

Type i polymeric MIECs incorporating proton conducting ionomers in acidic electrolytes reach very high σ_{ion} (10^{-2} - 10^{-1} S cm⁻¹, Figure 5), almost assuredly due to Grotthuss transport of protons through a hydrogen bonded network (67, 68). In PEDOT templated on sPPO the proton hopping activation energy in 1M sulfuric acid (34-72 meV) was over twenty times lower than the activation energy of chain dependent hopping in dry polyelectrolyte based MIECs. Highlighting the effect of the Grotthuss mechanism, in the same material Li⁺ conductivity was one tenth that of protons (68).

Many studies assume single ion transport between the MIEC and liquid electrolyte. Any additional mass transport has been ascribed to solvent transport. In the case of polyelectrolyte based MIECs (i, iii, v) this assumption is likely true as Donnan exclusion arising from the fixed polyelectrolyte charge should prevent transport of ions of the same charge as the polyelectrolyte. However, in polymer electrolyte based MIECs (ii, iv, vi) there is neither fixed ionic charge nor Donnan exclusion. Both anions and cations are in equilibrium between the liquid electrolyte and the MIEC, and single ion transport is at odds with experimental observations of dopant and counter ion uptake (69–71).

1.4.4. Hydrogel Ionic Transport

Both highly hydrated and electrolyte swollen polymeric MIECs are more accurately described as conductive hydrogels, which is an area of explicit research (72–75). In such hydrogels ionic transport is decoupled from polymer chain dynamics as continuous liquid pathways are available for ionic transport. Thus, engineering high σ_{ion} is unnecessary, instead maintaining a percolative path for effective electronic transport is the main design goal, as discussed below. By separately engineering the electronic transport pathways while maintaining liquid (void) spaces spanning the nano to meso scale there is considerable overlap between MIEC hydrogels and structured porous materials.(74)

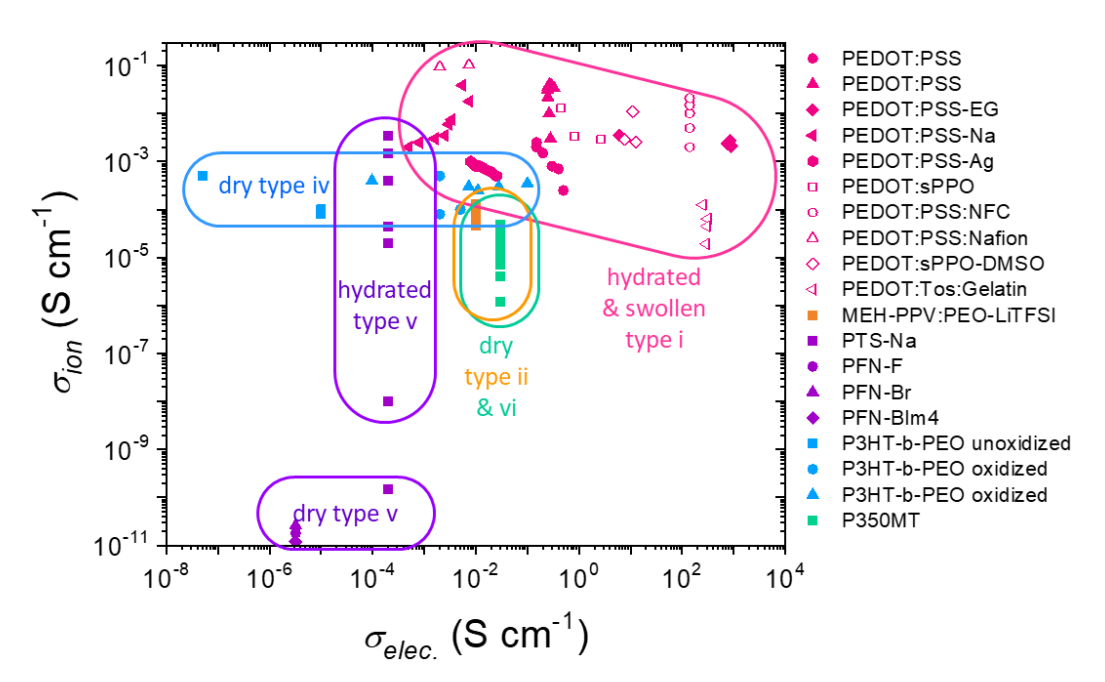


Figure 5. Ionic and electronic conductivity map of various types of polymeric MIECs under dry, hydrated, electrolyte swollen, and gelled conditions.

2. Electronic Transport in Polymeric MIECs

Of the extensive body of work studying electronic transport in CPs, the most insightful parallels to transport in polymeric MIECs can be drawn from the studies of molecular and electrochemically doped CPs. While molecular dopants ionize to donate electronic charge, electrochemical dopants are ions and tend to electrostatically stabilize electronic charge. Though both can occur in polymeric MIECs, electrochemical doping is especially important to consider due to the high ion

concentrations present. While the focus on CP-based systems reflects the state of the field, not all polymer MIECs are conjugated, see the side-bar on radical polymer MIECs to learn more.

Sidebar: Radical Polymers

As the name suggests, radical polymers can stabilize electronic charge not through conjugation and delocalization, but through stable open shell moieties, i.e. radicals. These radicals can couple with ions in a similar manner as electrochemical doping in CP-based MIECs (70), and their mixed conducting properties have made them attractive materials for battery electrodes (76). Ionic transport occurs in the same chain motion dependent manner as traditional polymer electrolytes. Radicals are often localized to pendant groups, and electronic transport occurs through self-exchange between pendant groups that are brought into close proximity via chain motion (77). In contrast to CPs, radical polymers do not require a rigid backbone for electronic transport. Instead, the same chain motion that imparts ionic conductivity also imparts electronic conductivity, with both showing a strong dependence on T_{α} (78).

2.1. Nature of Electronic Carriers

Just as ionic transport in polymeric MIECs requires the appropriate chemical functionality to solvate ions, electronic transport requires the proper electronic structure to stabilize mobile electronic charge carriers. This requisite electronic structure is most commonly achieved through extended conjugation that creates delocalized π -orbitals. Electronic carriers can be induced by adding an electron (reduction) or removing an electron to create a positively charged hole (oxidation). Following the nomenclature of semiconductors, polymeric MIECs that are readily oxidized and reduced are referred to as p-type and n-type materials, respectively, while those which undergo both are referred to as ambipolar.

While anions and cations in close proximity can form neutral pairs, unless the energetics are precisely engineered (79), an electron and hole in close proximity tend to recombine, annihilating both. Thus, it is unlikely to have areas of both sustained electron and hole concentration. Instead recombination zones form at the interface of n- and p-type regions, as exploited in LEECs (31).

The relative ease with which electronic carrier can be induced by molecular or electrochemical doping is directly related to the polymeric MIEC molecular orbitals energy level positions. To induce an electron the lowest occupied molecular orbital (LUMO) must be sufficiently deep, or to induce a hole the highest occupied molecular orbital (HOMO) must be sufficiently shallow to be

within accessible potentials for the given electrolyte system. For systems containing water, this range is ~4.0 to ~5.4 eV deep on the vacuum scale (80, 81).

Unlike crystalline inorganic materials where electronic charge carriers are nearly completely delocalized and interact little with the materials crystalline lattice, electronic carriers in polymeric MIECs are closely coupled to local structural deformation. It is useful to treat the electronic charge and coupled lattice deformation as a single quasi particle termed a polaron. Polarons themselves can combine into large quasiparticles to form bipolarons and multi polaronic/bipolaronic species (82).

Electroneutrality dictates that oppositely charged ions balance electronic carriers. The fixed polyelectrolyte charge in type i/iii/v materials can serve this function, while type ii/iv/vi materials require the injection of counter balancing dopant anions or cations. Alternatively, electronic carriers can be introduced into polymeric MIECs through molecular doping with molecules that favorably undergo charge transfer with polymeric MIECs. The same chemical functionality that allows polymeric MIECs to solvate ions, has also been found to improve molecular doping efficiency (83, 84).

2.2. Mechanism of Electronic Transport

As with ions, electrons and holes also move in response to applied field and concentration gradients. The drift-diffusion equation in one dimension gives the current density (J_n) for electrons:

$$J_n = en\mu_n \frac{d\phi}{dx} + enD_n \frac{dn}{dx}$$

and the current density (J_p) for holes:

$$J_p = ep\mu_p \frac{d\phi}{dx} + epD_p \frac{dp}{dx}$$

where n and p are the number densities, μ_n and μ_P are mobilities, and D_n and D_p are the diffusivities, for the electrons and holes, respectively. Thus, the n- and p-type electrical conductivity is given as $\sigma_n = en\mu_n$ and $\sigma_p = ep\mu_p$, respectively. Absent molecular doping, n and p are equal to the excess cation or anion concentrations, respectively. This is especially relevant in polymeric MIECs that are coupled with an external electrolyte and under potentiostatic control.

Electronic charge transport in doped CPs is often described as Efros–Shklovskii variable-range hopping (VRH) (27, 85, 86), where the electronic conductivity ($\sigma_{elec.}$) has the following temperature dependence.

$$\sigma_{elec.} = \sigma_{ES} e^{\left(\frac{T_{ES}}{T}\right)^{-\frac{1}{2}}}$$

Where σ_{ES} is the conductivity prefactor and T_{ES} is the characteristic temperature. The fundamental insight of this model is the presence of a Coulomb gap in the density of states (DOS) at the Fermi level. The Coulomb gap can be qualitatively rationalized as the energetic distance between the highest filled localized states (Fermi level) and the lowest empty delocalized states (transport level/mobility edge), Figure 6a inset. Increasing the charge density should decrease T_{ES} such and at or above T_{ES} , thermal energy should be sufficient to collapse the Coulomb gap resulting in high (metallic) conductivity (27). However this has not been unequivocally achieved (87), likely due to dopant induced disorder that accompanies high carrier densities (27).

Over smaller temperature ranges electronic mobility is commonly (if not strictly accurately) described as thermally activated hopping with an Arrhenius relationship:

$$\mu = \mu_0 e^{\left(\frac{-E_a}{RT}\right)}$$

$$\mu = \mu_0 \exp(-E_a/RT)$$

where the activation energy (E_a) and exponential prefactor (μ_0) are carrier density dependent. The activation energy is a useful parameter to approximate the difference between the Fermi level and transport level in order to compare the mobility at different carrier densities and in different materials (88, 89).

Efficient electronic transport in polymeric MIECs depends on particular characteristics on different length scales. On the shortest lengthscale, the degree of carrier localization is paramount. Decreased localization leads to lower activation energies and higher mobilities. Localization depends intrinsically on the chemical and molecular structure and extrinsically on the proximity of ions. Carriers can be localized to a particular repeat sub unit due to its electron accepting or donating character. Alternatively, large dihedral angles between repeat units can limit delocalization of charge to single (or few) repeat units. A classic CP example is regiorandom P3HT, where the steric hindrance of side chains in head-to-head coupled thiophenes introduces

significant torsion, decreasing the conjugation length and localizing charge, which widens the optical bandgap and decreases $\sigma_{elec.}$ (90, 91). In comparison, all head to tail coupled regioregular P3HT lacks this torsion and shows charge delocalization over 10 repeat units (92). This is reflected in the ℓ p of regiorandom (~10 Å) and regioregular (~29 Å) P3HT (35). When localization is the limiting factor, this leads to mixed valence redox transport where $\sigma_{elec.}$ maximums are observed in the half charged states (93). However, in most polymeric MIECs localization is not so extreme, and is one of several factors that affect electronic transport.

On longer length scales intrachain, interchain, and interdomain transport sum to produce macroscopic percolated electronic transport pathways. Low disorder (low torsion) that decreases carrier localization, also improves transport down the chain backbone (intra-chain transport). Planarity can be enhanced by backbone design or through intermolecular interactions (aggregation/crystallinity). Inherently planar backbones with fused rings or chemical functionality that limit torsion at single bond linkages (e.g. BBL, $\ell p \sim 1530$ Å) display low energetic disorder, independent of molecular packing (64, 94). In aggregates/crystallites, intermolecular interactions can force otherwise somewhat flexible chains into more ordered extended planar structures, more than doubling their ℓp (36) and extending charge carrier delocalization along the chain and onto neighboring chains (95), allowing efficient inter-chain transport. The extent of ordering can be just a few chains aggregated together up to crystallites 100s of nm in diameter, with increased aggregation/crystallinity generally correlatted with improved electronic transport. In the limit of very rigid planar polymers the minimum requisite aggregation for efficient inter-chain transport can be single close contacts between two chains (96).

The intermolecular aggregation/crystallinity that allows efficient interchain transport also produces discrete boundaries between crystallites and between crystalline and amorphous domains. Interdomain transport is impeded by the boundaries themselves and the high disorder of the amorphous regions (87). Doped CPs that show completely delocalized (metallic) carriers in ordered domains, still display thermally activated macroscopic transport due to these boundaries and amorphous regions (86). The effect of boundaries is minimized in films of highly rigid chains or aligned domains where boundaries are gradual and low angle (96, 97). Still, traversing the amorphous regions between crystallites requires individual connecting tie chains between crystallites/aggregates, Figure 6b. This results in a positive correlation between electronic transport and molecular weight, as longer chains more often bridge crystallites (98, 99). This is

exemplified in oligomeric MIECs that show much lower σ_{elec} than similar polymeric analogs (100, 101).

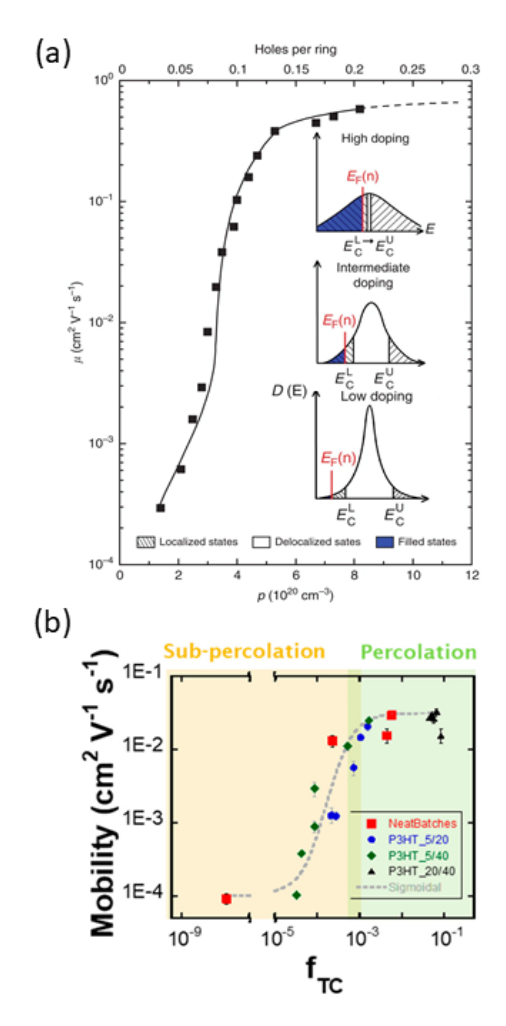


Figure 6. Electronic charge transport in the prototypical CP system P3HT: (a) doping dependent electronic mobility showing the dramatic rise and plateau with increased ionic dopant concentration adapted from (27), and (b) tie-chain dependent mobility in the prototypical CP P3HT demonstrating the critical fraction of tie-chains necessary for efficient electronic charge transport through a percolated network adapted from (99). The inset DOS diagrams in panel (a) shows the states filled up to the Fermi level (E_F) and the transport level (E_C), where the difference between E_F and E_C is the activation energy. The broadening effect of increased doping that localizes states and the shifts E_C frustrating the transition to a true band-like or metallic state.

2.3. Effect of lons on Electronic Transport

lons complicate electronic transport. At low concentrations ions present deep Coulomb wells that localize (trap) carriers and decrease their mobility (Figure 6a) (91, 102, 103), such that the carrier mobility in electrochemically doped devices is over an order of magnitude lower than in field effect devices at equivalent volumetric charge carrier density (88). Above ~0.1% doping (1 dopant ion per 1000 repeat units), electronic mobilities dramatically increase with increased dopant concentration as the tail of the DOS fills (Figure 6a) (103), and Coulomb wells overlap smoothing the energy landscape and reducing the hopping activation energy (89). This is reflected in an increased dielectric constant screening ions and carriers, and increased carrier localization lengths (27). High doping levels (~10%) leads to high mobilities (0.1-10 cm² V⁻¹ s⁻¹) and $\sigma_{elec.}$ (10-1000 S cm⁻¹) (85, 89, 104, 105), with hopping activation energies equivalent to the thermal energy (k_bT) at room temperature (88, 89). Above 10% doping, $\sigma_{elec.}$ improvements diminish with mobility plateauing as the cumulative disorder that accompanies doping flattens the DOS and decreases the number of delocalized transport states (Figure 6a inset) (27). At extreme doping levels, disorder is so great that carrier mobility is suppressed and $\sigma_{elec.}$ is extinguished (89).

2.4. Dry Electronic Transport

In dry type v materials, while total ion concentrations are high the dopant concentration (excess anion or cation) is well below 1% (49), and carrier mobility is quite low (~ 10^{-5} cm² V⁻¹ s⁻¹, Figure 5) (106). Type iv with balanced anion and cation concentrations also show quite low $\sigma_{elec.}$ (10^{-8} - 10^{-7} S cm⁻¹, Figure 5) but can be increased ~5 orders of magnitude by introducing excess dopants anions. Further, the dopant-conductivity relationship is not simply linear as a 10 fold increase in dopants yields a 100 fold increase in $\sigma_{elec.}$ (107). PEDOT:PSS (type i) is inherently highly doped (~30%) by the PSS⁻ on which it is templated. Additives or processing that remove superfluous PSS, improve domain purity, and create a well percolated network of PEDOT-rich domains yield $\sigma_{elec.} > 1000$ S cm⁻¹, Figure 5 (85, 104, 108).

2.5. Hydrated and Electrolyte Swollen Electronic Transport

In undoped CPs, water acts as an electronic trap diminishing electronic transport, and the displacement of water molecules from CP films drastically improves the electronic properties (109). Polymeric MIECs' high carrier densities can saturate such traps and their coordinating groups can potentially interact with water without creating traps, as they display high $\sigma_{elec.}$ in aqueous environments. The intrinsic and molecular doped $\sigma_{elec.}$ of conjugated polyelectrolytes (type v) is relatively insensitive to hydration (40, 50, 58). Similarly, high $\sigma_{elec.}$ formulations of

PEDOT:PSS (type i) are insensitive to hydration (58), while low $\sigma_{elec.}$ formulations show only a factor of 3 decrease in $\sigma_{elec.}$ at 100% RH (57).

When polymeric MIECs are in contact with a liquid electrolyte, the dopant density is directly tunable with electrochemical potential making them prime channel materials for organic electrochemical transistors (OECTs) (11, 110–113). The massive change in $\sigma_{elec.}$ with charge density permits high transconductance (gain), quantified in the intrinsic material figure of merit μC^* , the product of the charge carrier mobility and volumetric capacitance (reflecting the DOS) (114, 115).

Equilibrium between polymeric MIECs and liquid electrolytes leads to a strong dopant density dependence on electrolyte concentration and pH, in addition to electrochemical potential (61, 116, 117). The $\sigma_{elec.}$ of PEDOT:PSS is enhanced in acidic conditions, while increasing the pH decreases doping and increases in cation exchange, with sodium cations supplanting protons and preferentially associating with PSS⁻ (at the expense of holes on PEDOT) (118). This is reflected in PEDOT:PSSNa, which displays quite low $\sigma_{elec.}$ that is very sensitive to hydration (50, 58).

Inter-domain transport can be physically disrupted by the swelling that accompanies hydration and electrolyte exposure (50, 61, 62, 119). Monitoring crystallinity with in situ and ex situ X-ray scattering indicates that the bulk of the swelling must occur in the amorphous domains (26, 61, 120). Electronic transport should be especially sensitive to tie chains or domain contacts that create percolated pathways, Figure 6b. In conjugated polymer electrolytes (type vi) some swelling is necessary to facilitate dopant ion injection, but excessive swelling leads to decreases in carrier mobility (121–123).

2.6. Hydrogel Electronic Transport

When highly swollen, polymer MIECs are functionally hydrogels. Typically $\sigma_{elec.}$ is low, such that $\sigma_{elec.}$ approaching 10 S cm⁻¹ is considered ultra high (74, 124–126), reflecting the loss of percolation with swelling. $\sigma_{elec.}$ is inversely proportional to the degree of swelling in both PEDOT:PSS PEG/PAA double network and PEDOT:PSS single component hydrogels (75, 127). lons further disrupt percolation (likely screening electrostatic interactions between aggregates) as gelation with PBS reduces $\sigma_{elec.}$ 50% compared to gelation with water (75). Rheological analysis is common to hydrogel characterization (126), and given the expected connections between the

percolated electronic and mechanical network, combined rheological and electrical analysis is a promising avenue of study (128).

3. Ionic vs Electronic Transport

On the surface, the structural characteristics of efficient electronic transport (rigid chains, semicrystalline) seem at odds with characteristics of efficient ionic transport (flexible chains, amorphous). This holds in homogenous polymeric MIECs (v, vi), where the same backbone must impart electronic and ionic transporting characteristics and mixed transport requires a compromise of individual ionic and electronic transport (40, 47, 50, 129). Further, swelling that increases ionic transport, strains the percolated pathway of electronic transport. However, such compromises are largely sidestepped by separating the ionic and electronic transport into separate domains (i, ii, iii, iv). Dry type iv block copolymers show independently tuned ionic (via salt concentration) and electronic (via degree of oxidation) transport, Figure 5 (39, 45). Control of PEDOT:PSS (iv) morphology and hydration allows simultaneous high ionic and electronic conductivity (58, 59, 66, 68), with a 100 fold increase in electronic conductivity only diminishing ion diffusivities by a factor of two (104). For context, it is worth remembering that some of the highest electrical conductivities in polymers occur in mixed conducting materials (85, 108). Further, simply maximizing both is not the universal goal in polymer MIEC-based applications, instead it is the rational control of ionic and electronic transport. For instance, increased ionic transport leads to faster response times in LEECs (56), conversely decreased ionic transport leads to faster response times in organic light emitting diodes (130), and restraining ionic transport imparts non-volatility in synaptic-like devices (X. Ji, B.D. Paulsen, G.K.K. Chik, R. Wu, W.C.H. Choy, et al., manuscript in review). Given the wide variety of polymeric MIECs, there is likely the proper balance of mixed conducting properties to satisfy most every application.

4. Heat/energy transport in OMIECs

In addition to drift and diffusion, thermal gradients drive the transport (thermodiffusion) of both ionic and electronic charges. Additionally, mobile charge opens additional routes for heat transport. Thus, polymeric MIECs show unique thermodiffusion and thermal transport compared to pure electronically or ionically conducting polymers.

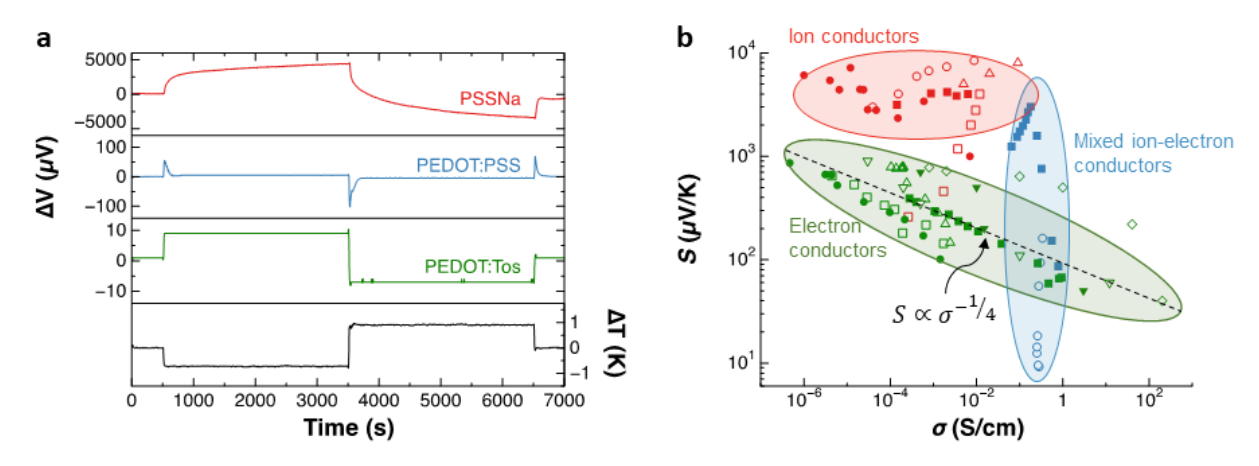


Figure 7. (a) Evolution of thermovoltage with time for a typical electron conductor (PEDOT:Tos), ion conductor (PSSNa) and mixed ion-electron conductor (PEDOT:PSS) at 80% RH, adapted with permission from (131). (b) Seebeck coefficient versus electrical conductivity for electron conductors (green), ion conductors (red) and mixed ion-electron conductors (blue), adapted with permission form (132). The empirical trend $S \propto \sigma^{-1/4}$ observed for electron conductors is shown for reference.

4.1. Seebeck coefficient

An applied thermal gradient (ΔT) drives thermodiffusion of charge carriers from hot to the cold (high to low entropy) ends establishing a steady-state thermovoltage (ΔV). Known as the Seebeck effect, the proportionality constant between ΔV and ΔT is the Seebeck coefficient ($S = -\Delta V/\Delta T$). Also known as thermopower, S is the entropy transported by a carrier divided by its charge, and represents a sum of contributions of the different charge carriers and their transport. For predominately electronic conductors (e.g., PEDOT:Tos) ΔV increases with increasing ΔT until saturating at a few tens or hundreds of $\mu V K^{-1}$ (94, 133, 134). Electronic carriers thermodiffuse quickly and the response of ΔV to ΔT is relatively fast (**Figure 7a**) (131). Conversely, in pure ionic conductors (e.g. PSSNa) ΔV is slow to reach steady state as ions thermodiffuse slowly due to the Soret effect. If only cations are mobile, as in the case of PSSNa, they will thermodiffuse faster than the immobile anions, accumulating at the cold end electrode. The resulting positive ΔV (~10 mV K⁻¹) is 1000× that of pure electronic conductors (135–137) and varies with ambient RH (58), as hydration enhances the thermodiffusion of the cations (**Figure 7a**).

In polymeric MIECs (e.g., PEDOT:PSS), the evolution of ΔV with ΔT is the result of two competing effects: ionic vs electronic thermodiffusion. Initially, cations accumulate at the cold end, and ΔV increases steadily as ΔT increases, reaching a maximum value of 0.1-1 mV K⁻¹ depending on RH.

This ionic transport changes the doping level locally throughout the sample (131), causing electronic and ionic carriers to re-distribute to ensure electroneutrality. This is accompanied by a decrease in ΔV to around 5-10 μ V/K, equivalent to the pure electronic contribution to ΔV (**Figure 7a**). Unlike the ionic contribution, the electronic contribution to ΔV is independent of the relative humidity (58). Because of its transient nature, this ionic Seebeck effect in MIECs does not contribute power generation, but can be exploited for simultaneous independent pressure-humidity-temperature sensing (137).

Mobile electrochemically active redox species and reactive electrodes allow continual thermogenerated ionic currents and constant power generation in polymeric MIECs. Ag⁺ electrochemically reacting with silver metal electrodes in PEDOT:Ag:PSS gives rise to a thermogalvanic effect (57). Holes are transported in the PEDOT-rich regions, while cations (Ag⁺ and/or protons) thermodiffuse preferentially within the PSS-rich domains, generating an extra constant current on top of the non-constant ionic Seebeck effect. The addition of pure ionic conductors like PSSH to polymeric MIECs results in hydrogels that are able to maintain the hydration necessary for effective ionic transport under ambient conditions, yielding stable thermopowers >15 mV K⁻¹ (138). The sign of the Seebeck coefficient can also be reversed from positive (mobile cations) to negative (mobile anions) by tailoring the ion/polymer matrix interaction (139, 140).

S and $\sigma_{elec.}$ of pure electronic conductors are interrelated as a function of the charge carrier concentration (*i.e.*, S decreases as σ increases). This behavior is typically rationalized in terms of energy of the carrier with respect to the chemical potential of the material. Upon doping, an increase in charge carrier concentration drives the Fermi level closer to the transport level such that the energy per carrier decreases. An empirical power law relationship between S and $\sigma_{elec.}$ (i.e., $S \propto \sigma_{elec.}^{-1/4}$) has been observed across a broad range of $\sigma_{elec.}$ and different pure electronic conductors (**Figure 7b**) (141). While the origin of this quasi-universal trend is yet to be understood, it is typically attributed to inhomogeneity in the polymeric film morphology (142) or energetic disorder due to the presence of ionized dopants (143). Structural anisotropy in crystalline polymers can induce both S and $\sigma_{elec.}$ to increase simultaneously (144), yielding power factor values ($S\sigma^2$) that go beyond those predicted by the empirical power law relationship.

Polymeric pure ion conductors do not typically follow this quasi-universal trend (**Figure 7b**). In polymeric ion gels, the σ_{ion} increases with increasing the ionic liquid content, while the ionic

Seebeck coefficient remains constant (139). In PSS, increased hydration increases the cation mobility (anions are immobile in PSS), without varying the ion concentration (145), simultaneously increasing both S and σ_{ion} , leading to an S vs σ relationship orthogonal to that of pure electronic conductors. A similar trend is reported for polymeric MIECs where conductivity is primarily dominated by humidity independent electronic transport, while the Seebeck coefficient is largely dominated by humidity dependent ionic thermodiffusion (**Figure 7b**) (58).

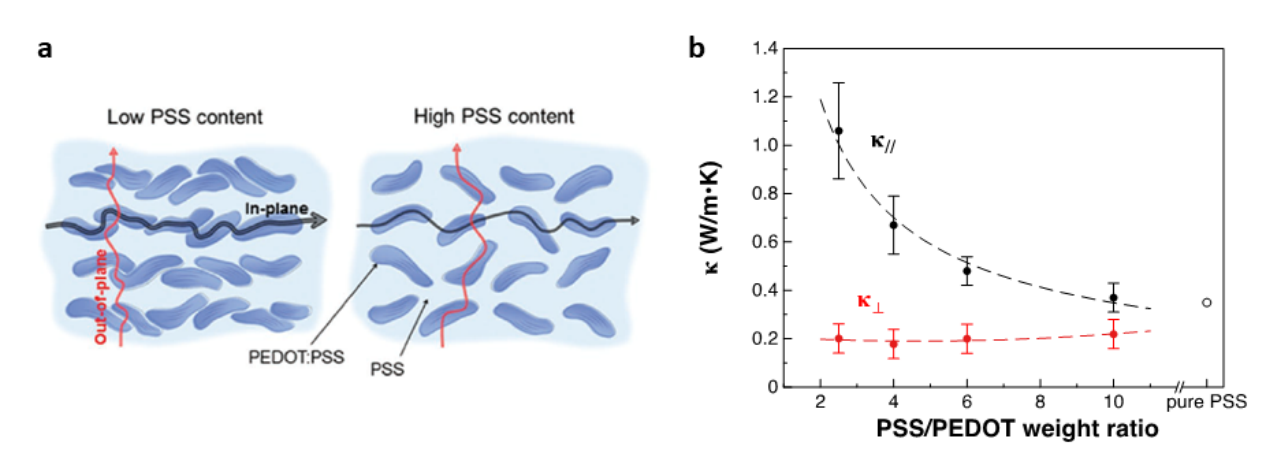


Figure 8. Similar to charge transport, (a) heat transport in PEDOT:PSS is fast along the in-plane direction and slow in the out-of-plane direction. (b) In-plane (black) and out-of-plane (red) thermal conductivity versus PSS load (κ for PSS taken from Reference (58)). Panel (a) and (b) adapted from (146).

4.2. Thermal conductivity

In electronic conductors, phonons and electrons contribute to heat transport and the resulting thermal conductivity (κ) , has a lattice (κ_L) and electronic (κ_{el}) component, such that $\kappa = \kappa_L + \kappa_{el}$. κ_{el} and $\sigma_{elec.}$ are related by the Wiedemann-Franz's law, $\kappa_{el} = LT\sigma_{elec.}$, where L is the Lorentz number. In CPs, κ_{el} is typically 0.1-0.5 W m⁻¹ K⁻¹, with κ_{el} becoming significant when $\sigma_{elec.}$ exceeds 10 S cm⁻¹ (147). As heat transport is more efficient through covalent bonding along the chain direction than through van der Waals interactions between chains, amorphous and ordered regions have different contributions to κ . In PEDOT:PSS, anisotropic phase separation results in anisotropic κ (148), with fast in-plane heat transport through interconnected (high $\sigma_{elec.}$) PEDOT-rich domains and slower PSS limited heat transport out of plane (**Figure 8a**) (149). This anisotropy vanishes with increased PSS loading and κ approaches that of pure PSS as in-plane $\sigma_{elec.}$ decreases and heat transport is limited by PSS in all directions (**Figure 8b**) (146).

Polyelectrolytes display a hydration dependent κ . In PSSNa, κ increases from 0.35 to 0.49 W m⁻¹ K⁻¹, when RH is increased from 50 to 100% (145). This rise is explained as the formation of parallel polymer-rich and aqueous-rich paths of thermal transport (κ_{H2O} =0.6 W m⁻¹ K⁻¹ at room temperature). Similar trends are reasonably expected in hydrated polymeric MIECs. Hydration should affect κ_L but not κ_{el} , as σ_{elec} is independent of hydration and σ_{ion} is typically less than 10⁻² S cm⁻¹ (58). To a first approximation, the thermal conductivity should be a composition-weighted average of the lattice contributions to the thermal conductivity of the solvent and of the conducting polymer. However, the empirical results are more complicated with high and low σ_{elec} . PEDOT:PSS showing opposite trends in κ with hydration (150). This complexity behavior calls for a better understanding of thermal transport in polymeric MIECs.

Conclusion

There exists a growing body of work studying mixed ionic and electronic transport in polymeric materials. Mixed ionic and electronic transport in polymers requires proper chemical functionality to solvate ions and stabilize electrons and/or holes. Ionic transport depends on chain motion, while electronic transport depends on intermolecular interactions and macroscopic percolation. This can be achieved with a variety of polymer blends, block copolymers, and homopolymers, each with their own strengths and weaknesses. The varied applications of polymeric MIECs require vastly different operating environments (dry, hydrated, electrolyte swollen, ect.), which leads to the same material displaying drastically different mixed conducting properties depending on environment. However, proper choice of polymer MIECs can provide efficient mixed transport irrespective of application environment. Studies thus far have focused on a limited range of materials (mostly PEDOT:PSS based), and quantitative reports of ionic transport are for the most part limited to type i and iv polymeric MIECs. Expanding ionic transport studies to a wider range of polymeric MIECs is needed. Processing additives for increased ionic transport in dry materials is currently neglected. Low disorder planar conjugated polymer electrolytes and polyelectrolytes have tantalizing potential for improved electronic charge transport. Polymeric MIECs are uniquely capable of simultaneously containing and transporting very high ionic and electronic charge carrier densities, and the coupling between these high ionic and electronic charge densities lies at the heart of their unique functionality. Better understanding of these ionic-electronic coupling properties is the key to advance the new applications. Interest in polymeric MIECs is spread across many fields, and improving mixed transport in particular polymeric MIEC types and applications requires leveraging the collective knowledge across disciplines. Further progress

across these fronts will improve the feasibility of polymeric MIECs in the many current areas of interest, and open new application areas for these exciting materials.

Acknowledgements

S. F. gratefully acknowledges support from the Swedish Research Council (2016-03979), Olle Engkvists Stiftelse (204-0256), and the Advanced Functional Materials Center at Linköping University (2009-00971). B.P. and J.R. gratefully acknowledge support from the National Science Foundation Grant No. NSF DMR-1751308. J.R gratefully acknowledge support from the Alfred P. Sloan Foundation.

Literature Cited

- Bolto BA, McNeill R, Weiss DE. 1963. Electronic Conduction in Polymers. III. Electronic Properties of Polypyrrole. Aust. J. Chem. 16(6):1090–1103
- Shirakawa H, Louis EJ, MacDiarmid AG, Chiang CK, Heeger AJ. 1977. Synthesis of electrically conducting organic polymers: halogen derivatives of polyacetylene, (CH)x. J. Chem. Soc., Chem. Commun., pp. 578–80
- Fenton DE, Parker JM, Wright PV. 1973. Complexes of alkali metal ions with poly(ethylene oxide). *Polymer*. 14(11):589
- 4. Wright PV. 1975. Electrical conductivity in ionic complexes of poly(ethylene oxide). *British Polymer Journal*. 7(5):319–27
- 5. Minett MG, Owen JR. 1988. Polymeric insertion electrodes. *Solid State Ionics*. 28–30:1192–96
- 6. Paulsen BD, Tybrandt K, Stavrinidou E, Rivnay J. 2020. Organic mixed ionic–electronic conductors. *Nature Materials*. 19(1):13–26
- 7. Costa RD, ed. 2017. Light-Emitting Electrochemical Cells: Concepts, Advances and Challenges. Springer International Publishing
- Melling D, Martinez JG, Jager EWH. 2019. Conjugated Polymer Actuators and Devices:
 Progress and Opportunities. Advanced Materials. 31(22):1808210

- 9. van de Burgt Y, Melianas A, Keene ST, Malliaras G, Salleo A. 2018. Organic electronics for neuromorphic computing. *Nature Electronics*. 1(7):386–97
- Zeglio E, Rutz AL, Winkler TE, Malliaras GG, Herland A. 2019. Conjugated Polymers for Assessing and Controlling Biological Functions. *Advanced Materials*. 31(22):1806712
- 11. Rivnay J, Inal S, Salleo A, Owens RM, Berggren M, Malliaras GG. 2018. Organic electrochemical transistors. *Nature Reviews Materials*. 3(2):17086
- Sjöström TA, Berggren M, Gabrielsson EO, Janson P, Poxson DJ, et al. 2018. A Decade of Iontronic Delivery Devices. Advanced Materials Technologies. 3(5):1700360
- Peterson KA, Thomas EM, Chabinyc ML. 2020. Thermoelectric Properties of Semiconducting Polymers. Annual Review of Materials Research. 50(1):551–74
- Meng Q, Cai K, Chen Y, Chen L. 2017. Research progress on conducting polymer based supercapacitor electrode materials. *Nano Energy*. 36:268–85
- Xie J, Gu P, Zhang Q. 2017. Nanostructured Conjugated Polymers: Toward High-Performance Organic Electrodes for Rechargeable Batteries. ACS Energy Lett. 2(9):1985–96
- Neo WT, Ye Q, Chua S-J, Xu J. 2016. Conjugated polymer-based electrochromics:
 materials, device fabrication and application prospects. *J. Mater. Chem. C.* 4(31):7364–76
- 17. Ratner MA, Shriver DF. 1988. Ion transport in solvent-free polymers. *Chem. Rev.* 88(1):109–24
- 18. Bruce PG, ed. 1994. Solid State Electrochemistry. Cambridge: Cambridge University Press
- Hallinan DT, Balsara NP. 2013. Polymer Electrolytes. Annual Review of Materials Research. 43(1):503–25
- 20. Choo Y, Halat DM, Villaluenga I, Timachova K, Balsara NP. 2020. Diffusion and migration in polymer electrolytes. *Progress in Polymer Science*. 103:101220

- Pace G, Friend R. 2013. Optical Processes in Conjugated Polyelectrolytes Dependence on Chain Conformation and Film Morphology. In *Conjugated Polyelectrolytes*, pp. 389–410.
 John Wiley & Sons, Ltd
- 22. Mai C-K, Schlitz RA, Su GM, Spitzer D, Wang X, et al. 2014. Side-Chain Effects on the Conductivity, Morphology, and Thermoelectric Properties of Self-Doped Narrow-Band-Gap Conjugated Polyelectrolytes. *J. Am. Chem. Soc.* 136(39):13478–81
- 23. Kee S, Haque MA, Lee Y, Nguyen TL, Rosas Villalva D, et al. 2020. A Highly Conductive Conjugated Polyelectrolyte for Flexible Organic Thermoelectrics. ACS Appl. Energy Mater.
- 24. Chevrier M, Kesters J, Houston JE, Brande NV den, Chambon S, et al. Phosphonium-based polythiophene conjugated polyelectrolytes with different surfactant counterions: thermal properties, self-assembly and photovoltaic performances. *Polymer International*. n/a(n/a):
- 25. Thomas EM, Brady MA, Nakayama H, Popere BC, Segalman RA, Chabinyc ML. 2018. X-Ray Scattering Reveals Ion-Induced Microstructural Changes During Electrochemical Gating of Poly(3-Hexylthiophene). Advanced Functional Materials. 28(44):1803687
- Bischak CG, Flagg LQ, Yan K, Rehman T, Davies DW, et al. 2020. A Reversible Structural Phase Transition by Electrochemically-Driven Ion Injection into a Conjugated Polymer. J. Am. Chem. Soc. 142(16):7434–42
- 27. Wang S, Ha M, Manno M, Daniel Frisbie C, Leighton C. 2012. Hopping transport and the Hall effect near the insulator–metal transition in electrochemically gated poly(3hexylthiophene) transistors. *Nature Communications*. 3(1):1210
- 28. Volkov AV, Wijeratne K, Mitraka E, Ail U, Zhao D, et al. 2017. Understanding the Capacitance of PEDOT:PSS. *Advanced Functional Materials*. 27(28):1700329

- Tybrandt K, Zozoulenko IV, Berggren M. 2017. Chemical potential

 –electric double layer coupling in conjugated polymer

 –polyelectrolyte blends. Science Advances.
 3(12):eaao3659
- Riess I. 2000. Polymeric mixed ionic electronic conductors. Solid State Ionics. 136–137(1–2):1119–30
- 31. van Reenen S, Kemerink M. 2017. Light-Emitting Electrochemical Cells: Mechanisms and Formal Description. In *Light-Emitting Electrochemical Cells: Concepts, Advances and Challenges*, ed RD Costa, pp. 3–45. Cham: Springer International Publishing
- 32. Hiemenz PC, Lodge TP, Lodge TP. 2007. *Polymer Chemistry*. CRC Press
- Lee H, Venable RM, MacKerell AD, Pastor RW. 2008. Molecular Dynamics Studies of Polyethylene Oxide and Polyethylene Glycol: Hydrodynamic Radius and Shape Anisotropy. *Biophysical Journal*. 95(4):1590–99
- 34. Weill G, Maret G. 1982. Magnetic birefringence of polystyrene sulphonate: Molecular weight and concentration dependence. *Polymer*. 23(13):1990–93
- McCulloch B, Ho V, Hoarfrost M, Stanley C, Do C, et al. 2013. Polymer Chain Shape of Poly(3-alkylthiophenes) in Solution Using Small-Angle Neutron Scattering.
 Macromolecules. 46(5):1899–1907
- 36. Alexiadis O, Mavrantzas VG. 2013. All-Atom Molecular Dynamics Simulation of Temperature Effects on the Structural, Thermodynamic, and Packing Properties of the Pure Amorphous and Pure Crystalline Phases of Regioregular P3HT. *Macromolecules*. 46(6):2450–67
- 37. Mirsakiyeva A, Hugosson HW, Crispin X, Delin A. 2017. Quantum Molecular Dynamical Calculations of PEDOT 12-Oligomer and its Selenium and Tellurium Derivatives. *Journal of Elec Materi*. 46(5):3071–75
- 38. Franco-Gonzalez JF, Zozoulenko IV. 2017. Molecular Dynamics Study of Morphology of Doped PEDOT: From Solution to Dry Phase. *J. Phys. Chem. B.* 121(16):4299–4307

- 39. Patel SN, Javier AE, Stone GM, Mullin SA, Balsara NP. 2012. Simultaneous Conduction of Electronic Charge and Lithium Ions in Block Copolymers. *ACS Nano*. 6(2):1589–1600
- 40. Merkle R, Gutbrod P, Reinold P, Katzmaier M, Tkachov R, et al. 2017. Mixed conductivity of polythiophene-based ionic polymers under controlled conditions. *Polymer*. 132:216–26
- Shiri P, Dacanay EJS, Hagen B, Kaake LG. 2019. Vogel–Tammann–Fulcher model for charging dynamics in an organic electrochemical transistor. *J. Mater. Chem. C*. 7(41):12935–41
- 42. Dong BX, Nowak C, Onorato JW, Strzalka J, Escobedo FA, et al. 2019. Influence of Side-Chain Chemistry on Structure and Ionic Conduction Characteristics of Polythiophene Derivatives: A Computational and Experimental Study. *Chem. Mater.* 31(4):1418–29
- 43. Chee KJ, Kumar V, Nguyen CV, Wang J, Lee PS. 2016. Polymer Light-Emitting

 Electrochemical Cell Blends Based on Selection of Lithium Salts, LiX [X =

 Trifluoromethanesulfonate, Hexafluorophosphate, and Bis(trifluoromethylsulfonyl)imide]

 with Low Turn-On Voltage. *J. Phys. Chem. C.* 120(21):11324–30
- 44. Javier AE, Patel SN, Hallinan DT, Srinivasan V, Balsara NP. 2011. Simultaneous Electronic and Ionic Conduction in a Block Copolymer: Application in Lithium Battery Electrodes. *Angewandte Chemie International Edition*. 50(42):9848–51
- Bhatt MP, Thelen JL, Balsara NP. 2015. Effect of Copolymer Composition on Electronic Conductivity of Electrochemically Oxidized Poly(3-hexylthiophene)-b-poly(ethylene oxide)
 Block Copolymers. Chem. Mater. 27(14):5141–48
- 46. Miller TF, Wang Z-G, Coates GW, Balsara NP. 2017. Designing Polymer Electrolytes for Safe and High Capacity Rechargeable Lithium Batteries. *Acc. Chem. Res.* 50(3):590–93
- Lévesque I, Bazinet P, Roovers J. 2000. Optical Properties and Dual Electrical and Ionic Conductivity in Poly(3-methylhexa(oxyethylene)oxy-4-methylthiophene). *Macromolecules*. 33(8):2952–57

- 48. Lin F, Wang Y, Lonergan M. 2008. Ion transport in polyacetylene ionomers. *Journal of Applied Physics*. 104(10):103517
- Collins SD, Mikhnenko OV, Nguyen TL, Rengert ZD, Bazan GC, et al. 2017. Observing Ion Motion in Conjugated Polyelectrolytes with Kelvin Probe Force Microscopy. *Advanced Electronic Materials*. 3(3):1700005
- Wieland M, Dingler C, Merkle R, Maier J, Ludwigs S. 2020. Humidity-Controlled Water
 Uptake and Conductivities in Ion and Electron Mixed Conducting Polythiophene Films.

 ACS Appl. Mater. Interfaces. 12(5):6742–51
- 51. Xue Z, He D, Xie X. 2015. Poly(ethylene oxide)-based electrolytes for lithium-ion batteries. *J. Mater. Chem. A.* 3(38):19218–53
- 52. Yang C, Sun Q, Qiao J, Li Y. 2003. Ionic Liquid Doped Polymer Light-Emitting Electrochemical Cells. *J. Phys. Chem. B.* 107(47):12981–88
- 53. Armel V, Rivnay J, Malliaras G, Winther-Jensen B. 2013. Unexpected Interaction between PEDOT and Phosphonium Ionic Liquids. *J. Am. Chem. Soc.* 135(30):11309–13
- 54. Nardes AM, Kemerink M, de Kok MM, Vinken E, Maturova K, Janssen RAJ. 2008.

 Conductivity, work function, and environmental stability of PEDOT:PSS thin films treated with sorbitol. *Organic Electronics*. 9(5):727–34
- Spyropoulos GD, Gelinas JN, Khodagholy D. 2019. Internal ion-gated organic electrochemical transistor: A building block for integrated bioelectronics. *Science Advances*. 5(2):eaau7378
- Cao Y, Pei Q, Andersson MR, Yu G, Heeger AJ. 1997. Light-Emitting Electrochemical
 Cells with Crown Ether as Solid Electrolyte. J. Electrochem. Soc. 144(12):L317
- 57. Chang WB, Fang H, Liu J, Evans CM, Russ B, et al. 2016. Electrochemical Effects in Thermoelectric Polymers. *ACS Macro Lett.* 5(4):455–59
- 58. Wang H, Ail U, Gabrielsson R, Berggren M, Crispin X. 2015. Ionic Seebeck Effect in Conducting Polymers. *Advanced Energy Materials*. 5(11):1500044

- 59. Malti A, Edberg J, Granberg H, Khan ZU, Andreasen JW, et al. 2016. An Organic Mixed Ion–Electron Conductor for Power Electronics. *Advanced Science*. 3(2):1500305
- 60. Amdursky N, Głowacki ED, Meredith P. 2019. Macroscale Biomolecular Electronics and lonics. *Advanced Materials*. 31(3):1802221
- 61. Savva A, Cendra C, Giugni A, Torre B, Surgailis J, et al. 2019. Influence of Water on the Performance of Organic Electrochemical Transistors. *Chem. Mater.* 31(3):927–37
- Gladisch J, Stavrinidou E, Ghosh S, Giovannitti A, Moser M, et al. 2020. Reversible Electronic Solid–Gel Switching of a Conjugated Polymer. *Advanced Science*.
 7(2):1901144
- Flagg LQ, Giridharagopal R, Guo J, Ginger DS. 2018. Anion-Dependent Doping and
 Charge Transport in Organic Electrochemical Transistors. *Chem. Mater.* 30(15):5380–89
- 64. Berry GC. 1978. Properties of an optically anisotropic heterocyclic ladder polymer (BBL) in dilute solution. *Journal of Polymer Science: Polymer Symposia*. 65(1):143–72
- 65. Li G, G. Pickup P. 2000. Ion transport in poly(3,4-ethylenedioxythiophene)–poly(styrene-4-sulfonate) composites. *Physical Chemistry Chemical Physics*. 2(6):1255–60
- 66. Stavrinidou E, Leleux P, Rajaona H, Khodagholy D, Rivnay J, et al. 2013. Direct

 Measurement of Ion Mobility in a Conducting Polymer. *Advanced Materials*. 25(32):4488–
 93
- 67. McFarlane SL, Day BA, McEleney K, Freund MS, Lewis NS. 2011. Designing electronic/ionic conducting membranes for artificial photosynthesis. *Energy Environ. Sci.* 4(5):1700–1703
- 68. Liu J, R. Davis N, S. Liu D, T. Hammond P. 2012. Highly transparent mixed electron and proton conducting polymer membranes. *Journal of Materials Chemistry*. 22(31):15534–39
- Ispas A, Peipmann R, Bund A, Efimov I. 2009. On the p-doping of PEDOT layers in various ionic liquids studied by EQCM and acoustic impedance. *Electrochimica Acta*.
 54(20):4668–75

- 70. Wang S, Li F, Easley AD, Lutkenhaus JL. 2019. Real-time insight into the doping mechanism of redox-active organic radical polymers. *Nature Materials*. 18(1):69–75
- 71. Flagg LQ, Bischak CG, Quezada RJ, Onorato JW, Luscombe ChristineK, Ginger DS.
 2020. P-Type Electrochemical Doping Can Occur by Cation Expulsion in a HighPerforming Polymer for Organic Electrochemical Transistors. ACS Materials Lett.
 2(3):254–60
- 72. Ghosh S, Inganäs O. 1999. Conducting Polymer Hydrogels as 3D Electrodes: Applications for Supercapacitors. *Advanced Materials*. 11(14):1214–18
- 73. Dai T, Qing X, Lu Y, Xia Y. 2009. Conducting hydrogels with enhanced mechanical strength. *Polymer*. 50(22):5236–41
- 74. Yao B, Wang H, Zhou Q, Wu M, Zhang M, et al. 2017. Ultrahigh-Conductivity Polymer Hydrogels with Arbitrary Structures. *Advanced Materials*. 29(28):1700974
- 75. Lu B, Yuk H, Lin S, Jian N, Qu K, et al. 2019. Pure PEDOT:PSS hydrogels. *Nature Communications*. 10(1):1043
- Wilcox DA, Agarkar V, Mukherjee S, Boudouris BW. 2018. Stable Radical Materials for Energy Applications. Annual Review of Chemical and Biomolecular Engineering. 9(1):83– 103
- 77. Sato K, Ichinoi R, Mizukami R, Serikawa T, Sasaki Y, et al. 2018. Diffusion-Cooperative Model for Charge Transport by Redox-Active Nonconjugated Polymers. *J. Am. Chem. Soc.* 140(3):1049–56
- 78. Yu I, Jeon D, Boudouris B, Joo Y. 2020. Mixed Ionic and Electronic Conduction in Radical Polymers. *Macromolecules*. 53(11):4435–41
- 79. Xu K, Sun H, Ruoko T-P, Wang G, Kroon R, et al. 2020. Ground-state electron transfer in all-polymer donor–acceptor heterojunctions. *Nature Materials*. 19(7):738–44
- 80. Sun H, Gerasimov J, Berggren M, Fabiano S. 2018. n-Type organic electrochemical transistors: materials and challenges. *J. Mater. Chem. C.* 6(44):11778–84

- Giovannitti A, Rashid RB, Thiburce Q, Paulsen BD, Cendra C, et al. 2020. Energetic Control of Redox-Active Polymers toward Safe Organic Bioelectronic Materials.
 Advanced Materials. 32(16):1908047
- 82. Zozoulenko I, Singh A, Singh SK, Gueskine V, Crispin X, Berggren M. 2019. Polarons,
 Bipolarons, And Absorption Spectroscopy of PEDOT. *ACS Appl. Polym. Mater.* 1(1):83–
 94
- 83. Kroon R, Kiefer D, Stegerer D, Yu L, Sommer M, Müller C. 2017. Polar Side Chains

 Enhance Processability, Electrical Conductivity, and Thermal Stability of a Molecularly p
 Doped Polythiophene. *Advanced Materials*. 29(24):1700930
- 84. Kiefer D, Kroon R, Hofmann AI, Sun H, Liu X, et al. 2019. Double doping of conjugated polymers with monomer molecular dopants. *Nature Materials*. 18(2):149–55
- 85. Shi H, Liu C, Jiang Q, Xu J. 2015. Effective Approaches to Improve the Electrical Conductivity of PEDOT:PSS: A Review. *Advanced Electronic Materials*. 1(4):1500017
- 86. Kang K, Watanabe S, Broch K, Sepe A, Brown A, et al. 2016. 2D coherent charge transport in highly ordered conducting polymers doped by solid state diffusion. *Nature Materials*. 15(8):896–902
- Fratini S, Nikolka M, Salleo A, Schweicher G, Sirringhaus H. 2020. Charge transport in high-mobility conjugated polymers and molecular semiconductors. *Nature Materials*. 19(5):491–502
- 88. Xia Y, Cho JH, Lee J, Ruden PP, Frisbie CD. 2009. Comparison of the Mobility–Carrier Density Relation in Polymer and Single-Crystal Organic Transistors Employing Vacuum and Liquid Gate Dielectrics. *Advanced Materials*. 21(21):2174–79
- Paulsen BD, Frisbie CD. 2012. Dependence of Conductivity on Charge Density and Electrochemical Potential in Polymer Semiconductors Gated with Ionic Liquids. *J. Phys. Chem. C.* 116(4):3132–41

- Stevens DM, Qin Y, Hillmyer MA, Frisbie CD. 2009. Enhancement of the Morphology and Open Circuit Voltage in Bilayer Polymer/Fullerene Solar Cells. J. Phys. Chem. C. 113(26):11408–15
- 91. Jiang X, Harima Y, Yamashita K, Tada Y, Ohshita J, Kunai A. 2002. Doping-induced change of carrier mobilities in poly(3-hexylthiophene) films with different stacking structures. *Chemical Physics Letters*. 364(5):616–20
- 92. Kuroda S, Marumoto K, Sakanaka T, Takeuchi N, Shimoi Y, et al. 2007. Electron-nuclear double-resonance observation of spatial extent of polarons in polythiophene and poly(3-alkylthiophene). *Chemical Physics Letters*. 435(4):273–77
- 93. Trefz D, Ruff A, Tkachov R, Wieland M, Goll M, et al. 2015. Electrochemical Investigations of the N-Type Semiconducting Polymer P(NDI2OD-T2) and Its Monomer: New Insights in the Reduction Behavior. *J. Phys. Chem. C*. 119(40):22760–71
- Wang S, Sun H, Ail U, Vagin M, Persson POÅ, et al. 2016. Thermoelectric Properties of Solution-Processed n-Doped Ladder-Type Conducting Polymers. *Adv. Mater.* 28(48):10764–71
- 95. Ghosh R, Pochas CM, Spano FC. 2016. Polaron Delocalization in Conjugated Polymer Films. *J. Phys. Chem. C*. 120(21):11394–406
- 96. Thomas TH, Harkin DJ, Gillett AJ, Lemaur V, Nikolka M, et al. 2019. Short contacts between chains enhancing luminescence quantum yields and carrier mobilities in conjugated copolymers. *Nature Communications*. 10(1):2614
- 97. Bucella SG, Luzio A, Gann E, Thomsen L, McNeill CR, et al. 2015. Macroscopic and high-throughput printing of aligned nanostructured polymer semiconductors for MHz large-area electronics. *Nature Communications*. 6(1):8394
- Himmelberger S, Vandewal K, Fei Z, Heeney M, Salleo A. 2014. Role of Molecular Weight
 Distribution on Charge Transport in Semiconducting Polymers. *Macromolecules*.

 47(20):7151–57

- Gu K, Snyder CR, Onorato J, Luscombe CK, Bosse AW, Loo Y-L. 2018. Assessing the Huang–Brown Description of Tie Chains for Charge Transport in Conjugated Polymers.
 ACS Macro Lett. 7(11):1333–38
- 100. Dong BX, Liu Z, Misra M, Strzalka J, Niklas J, et al. 2019. Structure Control of a π-Conjugated Oligothiophene-Based Liquid Crystal for Enhanced Mixed Ion/Electron Transport Characteristics. ACS Nano. 13(7):7665–75
- 101. Parr ZS, Rashid RB, Paulsen BD, Poggi B, Tan E, et al. 2020. Semiconducting Small Molecules as Active Materials for p-Type Accumulation Mode Organic Electrochemical Transistors. Advanced Electronic Materials. 6(6):2000215
- 102. Harima Y, Eguchi T, Yamashita K. 1998. Enhancement of carrier mobilities in poly(3-methylthiophene) by an electrochemical doping. *Synthetic Metals*. 95(1):69–74
- 103. Hulea IN, Brom HB, Houtepen AJ, Vanmaekelbergh D, Kelly JJ, Meulenkamp EA. 2004.
 Wide Energy-Window View on the Density of States and Hole Mobility in Poly(\$p\$-Phenylene Vinylene). Phys. Rev. Lett. 93(16):166601
- 104. Rivnay J, Inal S, Collins BA, Sessolo M, Stavrinidou E, et al. 2016. Structural control of mixed ionic and electronic transport in conducting polymers. *Nature Communications*. 7:11287
- 105. Kim S-M, Kim C-H, Kim Y, Kim N, Lee W-J, et al. 2018. Influence of PEDOT:PSS crystallinity and composition on electrochemical transistor performance and long-term stability. *Nature Communications*. 9(1):3858
- 106. Tordera D, Kuik M, Rengert ZD, Bandiello E, Bolink HJ, et al. 2014. Operational Mechanism of Conjugated Polyelectrolytes. J. Am. Chem. Soc. 136(24):8500–8503
- 107. Patel SN, Javier AE, Balsara NP. 2013. Electrochemically Oxidized Electronic and Ionic Conducting Nanostructured Block Copolymers for Lithium Battery Electrodes. ACS Nano. 7(7):6056–68

- 108. Kim N, Kee S, Lee SH, Lee BH, Kahng YH, et al. 2014. Highly Conductive PEDOT:PSS Nanofibrils Induced by Solution-Processed Crystallization. Advanced Materials. 26(14):2268–72
- 109. Nikolka M, Broch K, Armitage J, Hanifi D, Nowack PJ, et al. 2019. High-mobility, trap-free charge transport in conjugated polymer diodes. *Nature Communications*. 10(1):2122
- 110. Kergoat L, Piro B, Berggren M, Horowitz G, Pham M-C. 2012. Advances in organic transistor-based biosensors: from organic electrochemical transistors to electrolyte-gated organic field-effect transistors. *Anal Bioanal Chem.* 402(5):1813–26
- 111. Kim SH, Hong K, Xie W, Lee KH, Zhang S, et al. 2013. Electrolyte-Gated Transistors for Organic and Printed Electronics. *Advanced Materials*. 25(13):1822–46
- 112. Zeglio E, Inganäs O. 2018. Active Materials for Organic Electrochemical Transistors.

 Advanced Materials. 30(44):1800941
- 113. Moser M, Ponder JF, Wadsworth A, Giovannitti A, McCulloch I. 2019. Materials in Organic Electrochemical Transistors for Bioelectronic Applications: Past, Present, and Future. Advanced Functional Materials. 29(21):1807033
- 114. Inal S, Malliaras GG, Rivnay J. 2017. Benchmarking organic mixed conductors for transistors. *Nature Communications*. 8(1):1767
- 115. Friedlein JT, McLeod RR, Rivnay J. 2018. Device physics of organic electrochemical transistors. *Organic Electronics*. 63:398–414
- 116. Lin P, Yan F, Chan HLW. 2010. Ion-Sensitive Properties of Organic Electrochemical Transistors. *ACS Appl. Mater. Interfaces*. 2(6):1637–41
- 117. Romele P, Ghittorelli M, Kovács-Vajna ZM, Torricelli F. 2019. Ion buffering and interface charge enable high performance electronics with organic electrochemical transistors. Nature Communications. 10(1):3044
- 118. Mochizuki Y, Horii T, Okuzaki H. 2012. Effect of pH on Structure and Conductivity of PEDOT/PSS. *Transactions of the Materials Research Society of Japan*. 37(2):307–10

- 119. Savva A, Wustoni S, Inal S. 2018. Ionic-to-electronic coupling efficiency in PEDOT:PSS films operated in aqueous electrolytes. *J. Mater. Chem. C.* 6(44):12023–30
- 120. Paulsen BD, Wu R, Takacs CJ, Steinrück H-G, Strzalka J, et al. Time-Resolved Structural Kinetics of an Organic Mixed Ionic–Electronic Conductor. *Advanced Materials*.

 n/a(n/a):2003404
- 121. Giovannitti A, Maria IP, Hanifi D, Donahue MJ, Bryant D, et al. 2018. The Role of the Side Chain on the Performance of N-type Conjugated Polymers in Aqueous Electrolytes. Chem. Mater. 30(9):2945–53
- 122. Savva A, Hallani R, Cendra C, Surgailis J, Hidalgo TC, et al. 2020. Balancing Ionic and Electronic Conduction for High-Performance Organic Electrochemical Transistors. Advanced Functional Materials. 30(11):1907657
- 123. Moser M, Hidalgo TC, Surgailis J, Gladisch J, Ghosh S, et al. 2020. Side Chain Redistribution as a Strategy to Boost Organic Electrochemical Transistor Performance and Stability. Advanced Materials. 32(37):2002748
- 124. Yuk H, Lu B, Zhao X. 2019. Hydrogel bioelectronics. Chem. Soc. Rev. 48(6):1642–67
- 125. Zhang W, Feng P, Chen J, Sun Z, Zhao B. 2019. Electrically conductive hydrogels for flexible energy storage systems. *Progress in Polymer Science*. 88:220–40
- 126. Guo Y, Bae J, Fang Z, Li P, Zhao F, Yu G. 2020. Hydrogels and Hydrogel-Derived Materials for Energy and Water Sustainability. *Chem. Rev.*
- 127. Naficy S, Razal JM, Spinks GM, Wallace GG, Whitten PG. 2012. Electrically Conductive, Tough Hydrogels with pH Sensitivity. *Chem. Mater.* 24(17):3425–33
- 128. Newbloom GM, Weigandt KM, Pozzo DC. 2012. Electrical, Mechanical, and Structural Characterization of Self-Assembly in Poly(3-hexylthiophene) Organogel Networks.

 Macromolecules. 45(8):3452–62

- 129. Danielsen SPO, Sanoja GE, McCuskey SR, Hammouda B, Bazan GC, et al. 2018. Mixed Conductive Soft Solids by Electrostatically Driven Network Formation of a Conjugated Polyelectrolyte. Chem. Mater. 30(4):1417–26
- 130. Garcia A, Bakus II RC, Zalar P, Hoven CV, Brzezinski JZ, Nguyen T-Q. 2011. Controlling Ion Motion in Polymer Light-Emitting Diodes Containing Conjugated Polyelectrolyte Electron Injection Layers. J. Am. Chem. Soc. 133(8):2492–98
- 131. Ail U, Jafari MJ, Wang H, Ederth T, Berggren M, Crispin X. 2016. Thermoelectric Properties of Polymeric Mixed Conductors. *Adv. Funct. Mater.* 26(34):6288–96
- 132. Jiang Q, Sun H, Zhao D, Zhang F, Hu D, et al. High Thermoelectric Performance in n-Type Perylene Bisimide Induced by the Soret Effect. *Advanced Materials*. n/a(n/a):2002752
- 133. Bubnova O, Khan ZU, Malti A, Braun S, Fahlman M, et al. 2011. Optimization of the thermoelectric figure of merit in the conducting polymer poly(3,4-ethylenedioxythiophene). Nat Mater. 10(6):429–33
- 134. Patel SN, Glaudell AM, Peterson KA, Thomas EM, O'Hara KA, et al. 2017. Morphology controls the thermoelectric power factor of a doped semiconducting polymer. Science Advances. 3(6):e1700434
- 135. Zhao D, Fabiano S, Berggren M, Crispin X. 2017. Ionic thermoelectric gating organic transistors. *Nat Commun*. 8:
- 136. Li T, Zhang X, Lacey SD, Mi R, Zhao X, et al. 2019. Cellulose ionic conductors with high differential thermal voltage for low-grade heat harvesting. *Nature Materials*. 18(6):608–13
- 137. Han C-G, Qian X, Li Q, Deng B, Zhu Y, et al. 2020. Giant thermopower of ionic gelatin near room temperature. *Science*. 368(6495):1091–98
- 138. Kim B, Na J, Lim H, Kim Y, Kim J, Kim E. 2019. Robust High Thermoelectric Harvesting

 Under a Self-Humidifying Bilayer of Metal Organic Framework and Hydrogel Layer.

 Advanced Functional Materials. 29(7):1807549

- 139. Zhao D, Martinelli A, Willfahrt A, Fischer T, Bernin D, et al. 2019. Polymer gels with tunable ionic Seebeck coefficient for ultra-sensitive printed thermopiles. *Nature Communications*. 10(1):1093
- 140. Kim B, Hwang JU, Kim E. 2020. Chloride transport in conductive polymer films for an n-type thermoelectric platform. *Energy Environ. Sci.* 13(3):859–67
- 141. Glaudell AM, Cochran JE, Patel SN, Chabinyc ML. 2015. Impact of the Doping Method on Conductivity and Thermopower in Semiconducting Polythiophenes. *Advanced Energy Materials*. 5(4):1401072
- 142. Kang SD, Snyder GJ. 2017. Charge-transport model for conducting polymers. *Nature Materials*. 16(2):252–57
- 143. Abdalla H, Zuo G, Kemerink M. 2017. Range and energetics of charge hopping in organic semiconductors. *Phys. Rev. B.* 96(24):241202
- 144. Scheunemann D, Vijayakumar V, Zeng H, Durand P, Leclerc N, et al. 2020. Rubbing and Drawing: Generic Ways to Improve the Thermoelectric Power Factor of Organic Semiconductors? Advanced Electronic Materials. 6(8):2000218
- 145. Wang H, Zhao D, Khan ZU, Puzinas S, Jonsson MP, et al. 2017. Ionic Thermoelectric Figure of Merit for Charging of Supercapacitors. Advanced Electronic Materials. 3(4):1700013
- 146. Håkansson A, Shahi M, Brill JW, Fabiano S, Crispin X. 2019. Conducting-Polymer Bolometers for Low-Cost IR-Detection Systems. Advanced Electronic Materials. 5(6):1800975
- 147. Weathers A, Khan ZU, Brooke R, Evans D, Pettes MT, et al. 2015. Significant Electronic Thermal Transport in the Conducting Polymer Poly(3,4-ethylenedioxythiophene). Adv. Mater. 27(12):2101–6

- 148. Liu J, Wang X, Li D, Coates NE, Segalman RA, Cahill DG. 2015. Thermal Conductivity and Elastic Constants of PEDOT:PSS with High Electrical Conductivity. *Macromolecules*. 48(3):585–91
- 149. Wei Q, Mukaida M, Kirihara K, Ishida T. 2014. Experimental Studies on the Anisotropic Thermoelectric Properties of Conducting Polymer Films. *ACS Macro Lett.* 3(9):948–52
- 150. Kim G-H, Kim J, Pipe KP. 2016. Humidity-dependent thermoelectric properties of poly(3,4-ethylenedioxythiophene):poly(styrene sulfonate). *Appl. Phys. Lett.* 108(9):093301